

Chapter 5

The Optoelectronic Swept-Frequency Laser

5.1 Introduction

In this chapter, we study the application of the feedback techniques developed in the previous chapters to control the frequency of an SCL as it is tuned across a wide frequency range. As described in chapter 1, such broadband sources are important in many upcoming fields such as FMCW imaging and LIDAR, sensing and spectroscopy. The key requirements in these applications are rapid tuning over a broad frequency range, also referred to as the “chirp bandwidth,” and the precise control of the frequency chirp profile. The wide gain bandwidth of the semiconductor quantum well media, the narrow linewidth of a single-mode SCL, and the ability to electronically control the lasing frequency using the injection current make the SCL an attractive candidate for a wideband swept-frequency source for FMCW imaging. However, the bandwidth and the speed of demonstrated linear frequency sweeps have been limited by the inherent nonlinearity of the frequency modulation response of the SCL vs. the injection current, especially at high speeds. A feedback system to overcome this nonlinearity using a fiber interferometer and a lock-in technique has been reported [112]; however the rate of the frequency sweep was limited to about 100 GHz in 10 ms.

In this chapter, we report the development of an optoelectronic swept-frequency laser with precise control over the optical frequency sweep. The output frequency

of the SCL is a function of its driving current, and is controlled electronically by a combination of two techniques: (i) an open-loop predistortion of the input current into the SCL, and (ii) an optoelectronic feedback loop in which the optical chirp rate is phase-locked to a reference electronic signal. When the system is in lock, the slope and starting frequency of the optical frequency sweep are determined by the frequency and phase of the reference signal, and the laser emits a precise and coherent, predetermined ω vs. t waveform (“chirp”). This chirp is determined by the elements, both optical and electronic, of the feedback circuit and does not depend on the specific laser. The dynamic coherent control of the output frequency of an SCL opens up the field of SCL optics to many important applications such as chirped radar, biometrics, swept source spectroscopy, microwave photonics, and Terahertz imaging and spectroscopy.

Using a high coherence monochromatic reference oscillator in the optoelectronic feedback loop, we demonstrate rapid, highly linear frequency sweeps of up to 500 GHz in 100 μ s using DFB SCLs and VCSELs. Further, the frequency of the reference signal can varied dynamically to achieve arbitrary, time-varying optical frequency chirps. We demonstrate quadratic and exponential sweeps of the frequency of the SCL by varying the frequency of the reference signal. We report the results of label-free biomolecular sensing experiments using a precisely controlled SFL and whispering-gallery microtoroid resonators.

5.2 System Description

The feedback system for the generation of linear frequency chirps is shown in figure 5.1. A small part of the output of the fiber-coupled swept SCL is coupled into the feedback loop using a 10/90 fiber coupler. The optical signal is passed through a fiber Mach-Zehnder interferometer (MZI) with a differential time delay τ , and is incident on a photodetector (PD). When the optical frequency is varied with time, the frequency of the generated photocurrent is proportional to the slope of the optical frequency chirp. The output of the PD is mixed down using a reference signal of frequency ω_R ,

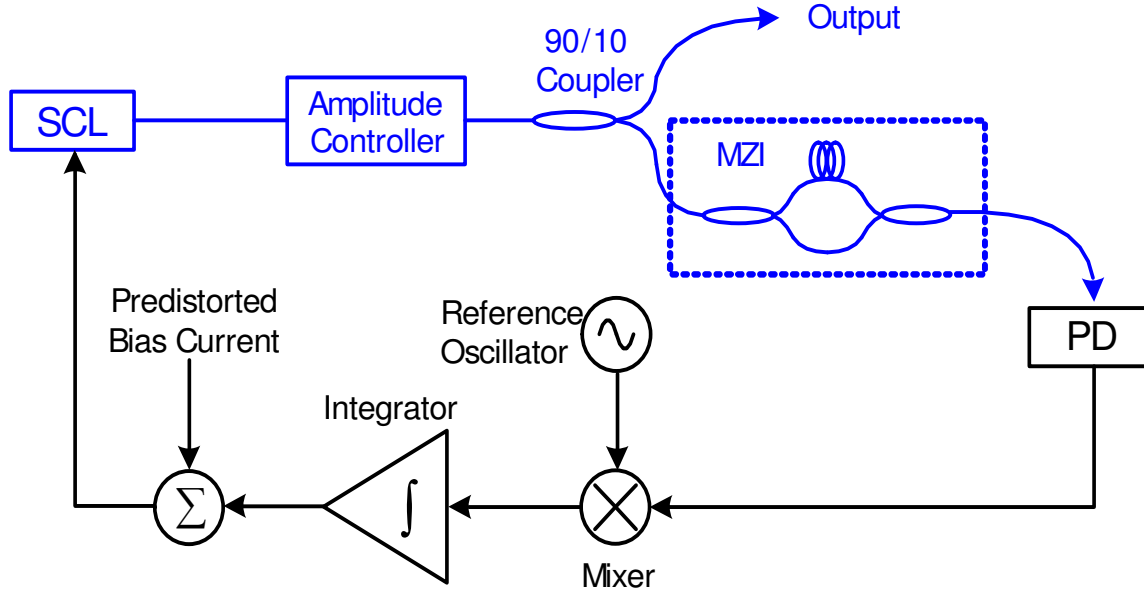


Figure 5.1. Optoelectronic feedback loop for the generation of accurate broadband linear chirps. The optical portion of the loop is shown in blue.

integrated, and injected into the SCL. Since the injection current into the SCL also modulates the optical power, a low-speed amplitude controller is used to maintain a constant output power. A bias current is added to the SCL to set the nominal optical frequency slope, and to provide an open-loop predistortion as described in section 5.2.2. The system is reset so that the chirp repeats every T seconds.

The steady-state solution of the control system is derived below. We start by demonstrating that a linear optical frequency chirp is a self-consistent solution. Let us assume that the laser frequency tuning is perfectly linear, and that there is no predistorted bias current present. Assume that the laser frequency is given by

$$\omega_{SCL}(t) = \omega_0 + \xi t, \quad (5.1)$$

where ξ is the slope of the optical frequency sweep. This corresponds to an optical phase

$$\phi(t) = \phi_0 + \omega_0 t + \frac{1}{2}\xi t^2. \quad (5.2)$$

The output of the photodetector PD is given by

$$i_{PD} = K_P \cos(\phi(t) - \phi(t - \tau)), \quad (5.3)$$

where the PD gain K_P is the product of the optical power and the PD responsivity, and we have ignored the DC term in the PD output. With the assumed chirp shape in equation (5.2), equation (5.3) describes a sinusoidally varying photocurrent with frequency

$$\omega_{PD} = \xi\tau. \quad (5.4)$$

The output of the mixer is

$$i_M = K_P K_M \cos(\phi(t) - \phi(t - \tau) - \omega_R t - \phi_R), \quad (5.5)$$

where K_M is the mixer gain, and the reference oscillator has a frequency ω_R and phase ϕ_R . Now let ω_R be chosen so that

$$\omega_R = \omega_{PD} = \xi\tau. \quad (5.6)$$

The mixer output is then a DC signal given by

$$i_M = K_P K_M \cos\left(\omega_0\tau - \frac{1}{2}\xi\tau^2\right). \quad (5.7)$$

This DC current is amplified and integrated to provide a linear (i vs. t) current to the laser, which in turn produces a frequency output as given by equation (5.1), thus providing a self-consistent solution.

More rigorously, the steady-state solution is obtained by requiring that the output current from the mixer in equation (5.5) is a constant, which means that

$$\frac{d}{dt}(\phi(t) - \phi(t - \tau)) = \omega_R. \quad (5.8)$$

The solution to equation (5.8) is determined by the initial laser frequency chirp, i.e.,

by the value of the optical frequency over the interval $[-\tau, 0]$. If the MZI delay τ is chosen sufficiently small so that the effect of higher-order derivatives of the optical frequency can be neglected, equation (5.8) reduces to

$$\tau \frac{d\omega_{SCL}}{dt} = \omega_R, \quad (5.9)$$

the solution to which is a linear frequency chirp as given by equation (5.1). Another way to look at the control system is as follows: the combination of the integrator, semiconductor laser, the MZI (which acts as a differentiator) and the PD act as a VCO, since the frequency of the PD output is proportional to the input voltage into the loop integrator. This VCO is locked to the reference oscillator in a typical Type I homodyne phase-locked loop. If we ignore the steady-state phase error in the loop—which is true if the loop gain is high, or the open-loop bias of the laser produces a nearly linear chirp—the slope and starting frequency of the optical chirp are given by

$$\begin{aligned} \xi &= \frac{\omega_R}{\tau}, \\ \omega_0 &= \frac{\phi_R + 2m\pi}{\tau}, \end{aligned} \quad (5.10)$$

where m is an integer. The steady-state solution of the system is therefore a set of linear optical frequency chirps, whose starting frequencies differ by the free-spectral range of the MZI. One of these solutions is picked out by the temperature and bias current of the SCL.

5.2.1 Small-Signal Analysis

The transient response of the system about the steady-state solution described by equation (5.10) is studied in the Fourier domain using the small-signal approximation as shown in figure 5.2. The variable in the loop is (the Fourier transform of) the deviation of the optical phase from its steady-state value in equation (5.10). For frequencies much smaller than its free spectral range, the MZI can be approximated as an ideal frequency discriminator. K denotes the total DC loop gain, given by the

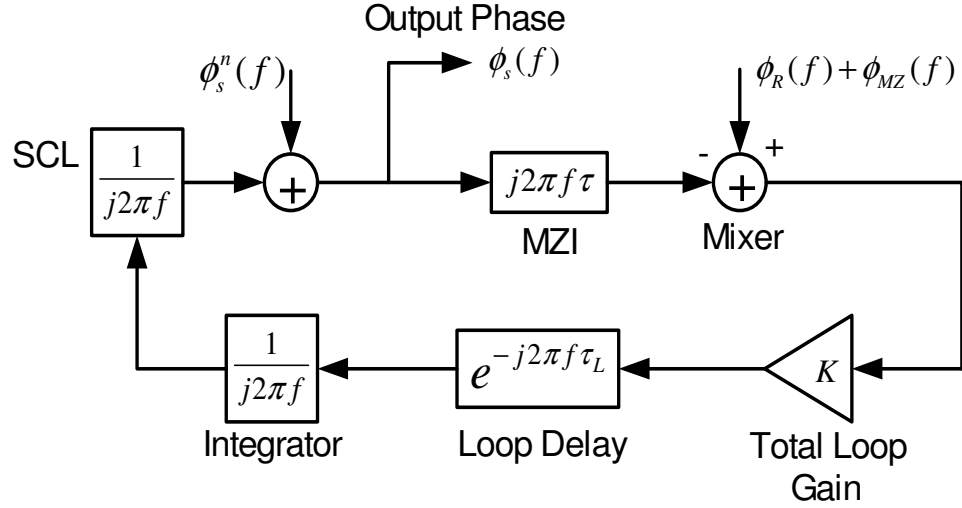


Figure 5.2. Small-signal phase propagation in the optoelectronic SFL feedback loop.

product of the gains of the laser, PD, mixer and the integrator. The phase noise of the laser and the phase excursion due to the nonlinearity of the frequency-vs.-current response of the SCL are lumped together and denoted by $\phi_s^n(f)$. The phase noise of the reference oscillator and the phase noise introduced by environmental fluctuations in the MZI are denoted by $\phi_R(f)$ and $\phi_{MZ}(f)$ respectively. Following a standard small-signal analysis [2], the output phase of the SCL is given by

$$\phi_s(f) = \phi_s^n(f) \frac{j2\pi f}{j2\pi f + K\tau e^{-j2\pi f\tau_L}} + (\phi_R(f) + \phi_{MZ}(f)) \frac{K\tau e^{-j2\pi f\tau_L}}{j2\pi f (j2\pi f + K\tau e^{-j2\pi f\tau_L})}, \quad (5.11)$$

where τ_L is the loop propagation delay. The nonlinearity and laser phase noise within the loop bandwidth are suppressed by the loop, as seen from the first term in equation (5.11). The frequency components of the nonlinearity are of the order of the repetition frequency of the waveform, and lie within the loop bandwidth. The analysis predicts the reduction in the phase noise of the SCL and an improvement in coherence, leading to a higher signal-to-noise ratio in an FMCW interferometric experiment (as described in chapter 3). From the second term in equation (5.11), we see that the accuracy of the frequency chirp is dependent on the frequency stability of the electronic oscillator used to generate the reference signal, and on the stability of the MZI. It is possible to obtain very accurate linear frequency chirps with the use of ultralow phase noise

electronic oscillators and stabilized optical interferometers.

5.2.2 Predistortion of the SCL Bias Current

The small-signal approximation of the preceding section is valid as long as the phase change introduced at the PD output due to nonlinearities in the tuning response of the SCL is small. This condition is satisfied if the differential delay τ in the MZI is small and the SCL nonlinearity is limited. However, the tuning response of the SCL is inherently nonlinear, since the predominant tuning mechanism is a current-induced temperature change which in turn changes the refractive index of the lasing medium. This nonlinearity is especially pronounced at higher sweep rates, and can throw the loop out of lock. The sweep nonlinearity can be reduced by predistorting the open-loop input current to the SCL, as follows. The frequency of the SCL is related to the input sweep current according to

$$\omega_{SCL}(t) = \omega_0 + K_{SCL}(i) \times i(t), \quad (5.12)$$

where the nonlinearity of the modulation response is modeled by a current-dependent gain $K_{SCL}(i)$. From equation (5.3), this generates a photocurrent at the PD which has a (in general, time-varying) frequency

$$\begin{aligned} \omega_{PD}(t) = \tau \frac{d\omega_{SCL}}{dt} &= \frac{di}{dt} \times \left(\tau K_{SCL} + \tau i \frac{dK_{SCL}}{di} \right) \\ &\doteq \frac{di}{dt} \times F_{dist}(i), \end{aligned} \quad (5.13)$$

where we have defined a “distortion function” $F_{dist}(i)$ that is a function of only the laser injection current.

We now develop a predistortion technique based on equation (5.13). A current ramp is applied to the SCL, the resultant PD frequency $\omega_{PD}(t)$ is measured, and the distortion function $F_{dist}(i)$ is extracted from this measurement. Next, this function is used to solve equation (5.13) numerically, and the predistorted current $i_{pre}(t)$ that results in the desired (here, a constant) $\omega_{PD}(t)$ is obtained.

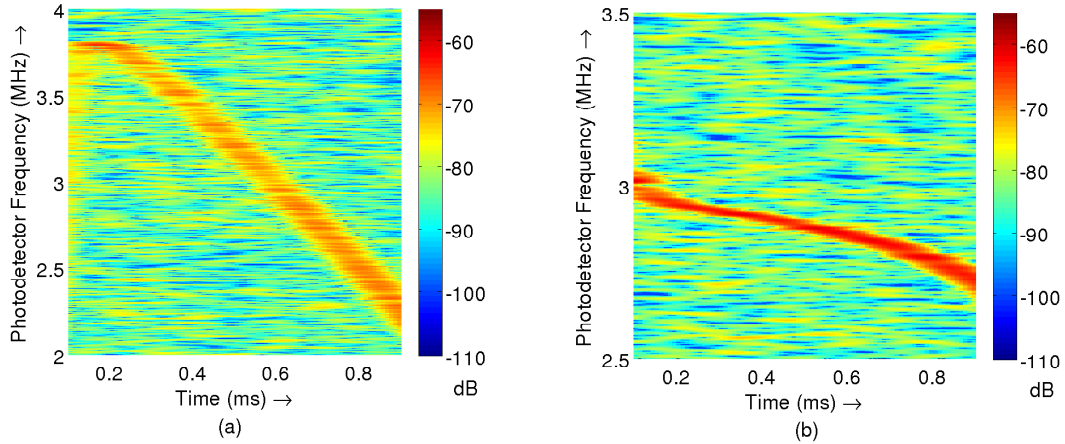


Figure 5.3. Measured spectrograms of the output of the loop photodetector, for the (a) free-running and (b) predistorted cases. The predistortion significantly reduces the SCL nonlinearity. The delay of the MZI is $\tau = 28.6$ ns.

The ability of the predistortion of the input current to significantly reduce the nonlinearity and enable phase-locking over a large frequency range is demonstrated in figure 5.3. The optical frequency chirp is characterized by measuring the frequency of the PD, ω_{PD} , since this is directly proportional to the slope of the frequency chirp as given by equation (5.4).¹ The measurements in figure 5.3 were performed using a DFB SCL (JDS-Uniphase) with an MZI delay of $\tau = 28.6$ ns. Panel (a) shows the spectrogram of the optical chirp slope when a constant current ramp is applied to the SCL, and panel (b) corresponds to the predistorted input. Note that the loop is not closed, i.e. $K = 0$, in these measurements. It is clearly seen that the nonlinearity of the chirp, as characterized by the spread of frequencies in the photocurrent spectrogram, is clearly reduced by the predistortion.

While the predistortion significantly reduces the chirp nonlinearity, it does not eliminate it, as seen in figure 5.3(b). This is due to the fact that the assumed model for the laser nonlinearity (equation (5.12)) is only approximate. The tuning coefficient K_{SCL} is not merely a function of the current i , but also of the rate of change of current, and possibly higher derivatives. Instead of coming up with a more complicated model

¹The measurements in figure 5.3 are the spectrograms of the photocurrent. A spectrogram is a moving-windowed Fourier transform of the input signal; it effectively measures the variation of the frequency of the signal as a function of time.

of the laser tuning behavior, we simply apply the predistortion technique iteratively, and it is observed that the laser nonlinearity all but vanishes after 3–4 iterations. The success of the iterative approach can be understood by noting that the calculated predistorting current approaches the required predistortion more closely with each iteration, and makes the model in equation (5.12) more and more accurate.

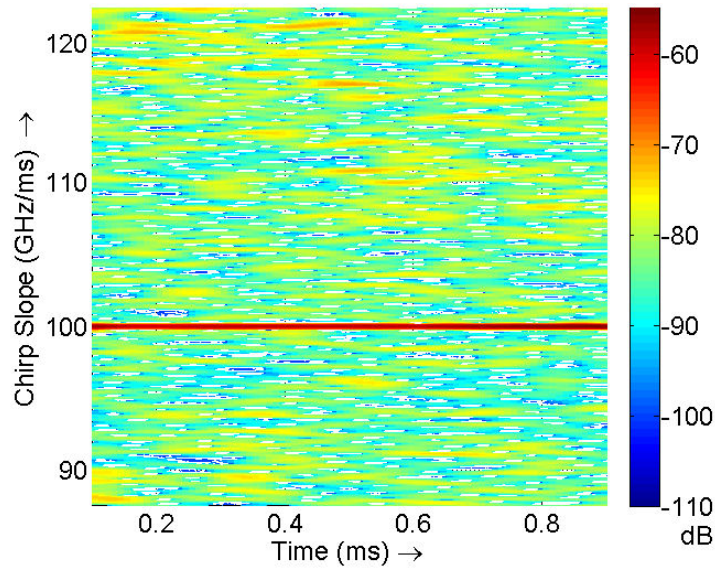
5.3 Experimental Demonstration

Experimental demonstrations of the control system shown in figure 5.1 were performed using various commercially available fiber-coupled SCLs at different wavelengths. We present here results using a DFB SCL (JDS-Uniphase) with an output power of 40 mW at a wavelength of 1539 nm and a VCSEL (RayCan, Daejeon, Korea) with an output power of 1 mW at 1550 nm. The delay in the fiber MZI, τ , was chosen to be as large as possible while remaining much smaller than the coherence time of the laser.

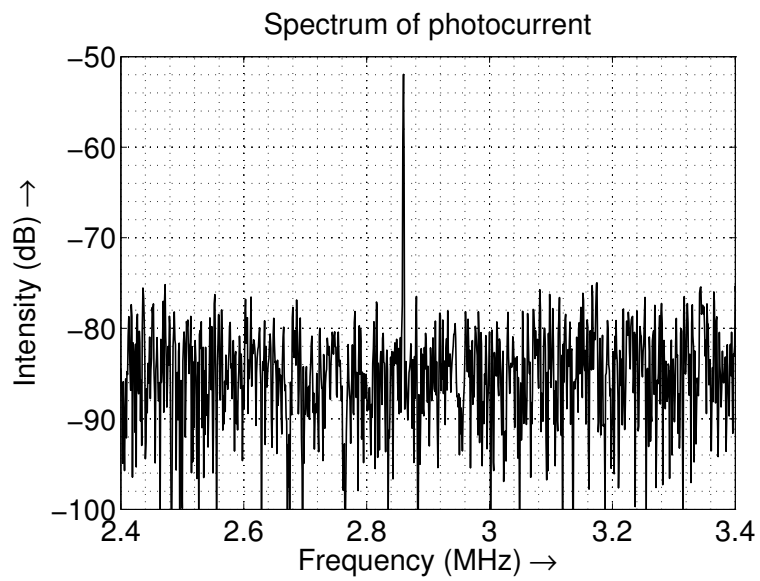
5.3.1 Linear Frequency Sweep

5.3.1.1 Distributed Feedback SCL

A perfectly linear chirp of 100 GHz in 1 ms was demonstrated using the DFB SCL, corresponding to a chirp slope of 10^{14} Hz/s. The MZI delay was $\tau = 28.6$ ns, so that the chirp rate of 10^{14} Hz/s corresponded to a photocurrent frequency $\omega_{PD}/2\pi = 2.86$ MHz. The measured spectrograms of the photocurrent for a ramped current bias and after predistortion are shown in figure 5.3. The predistorted frequency sweep was then locked to a high coherence external reference signal of frequency 2.86 MHz, to obtain a highly linear optical frequency sweep of 100 GHz in 1 ms. The loop gain was adjusted by varying the amplitude of the reference signal. A loop bandwidth of ± 200 kHz was achieved. The spectrogram of the PD current when the loop was in lock is plotted in figure 5.4(a), showing that the rate of the optical frequency sweep remains constant with time. The Fourier transform of the PD current, calculated



(a)



(b)

Figure 5.4. Measured spectrogram of the output of the loop photodetector when the loop is in lock, showing a perfectly linear optical chirp with slope 100 GHz/ms. (b) Fourier transform of the photodetector output measured over a 1 ms duration.

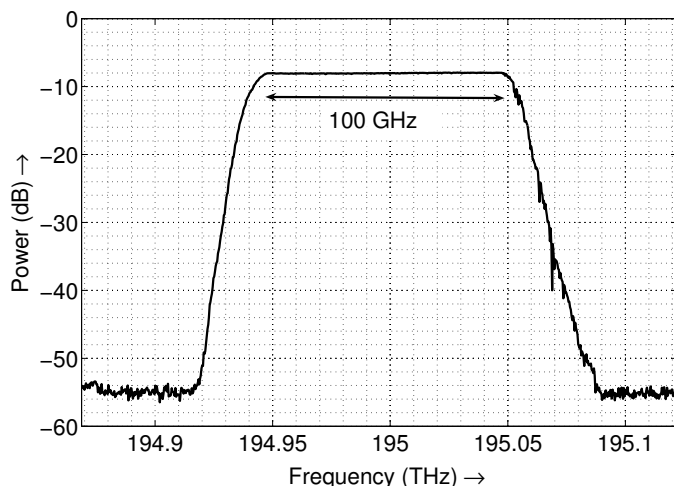


Figure 5.5. Measured optical spectrum of the locked swept-frequency SCL. RBW = 10 GHz.

over 1 ms and shown in Fig 5.4(b), shows a narrow peak at the reference frequency of 2.86 MHz. The width of the peak is transform-limited to 1 kHz. The spectrum of the swept laser measured using an optical spectrum analyzer is shown in figure 5.5.

5.3.1.2 Vertical Cavity Surface-Emitting Laser

The range of the frequency sweep in the experimental demonstration using the DFB SCL was limited by the tuning range of the laser. Single-mode VCSELs have larger tuning ranges, and we therefore performed the same experiment with single-mode VCSELs at 1550 nm. Further, the tuning speed was increased so that the scan time was 0.1 ms. The results of the experiment are summarized in figure 5.6. Panel (a) shows the shape of the optical chirp when a current ramp is applied to the VCSEL, and the tuning is highly nonlinear. The shape of the frequency sweep after four rounds of iterative predistortion is shown in panel (b), and it can be seen that the chirp is already very linear. A transform-limited peak is seen for this case. When the SCL is phase-locked, as in (c), any residual nonlinearities are corrected, and the starting frequency of the optical chirp is locked to the reference oscillator. The spectrum of the swept laser, shown in (d) verifies that the tuning range achieved is equal to 500 GHz.

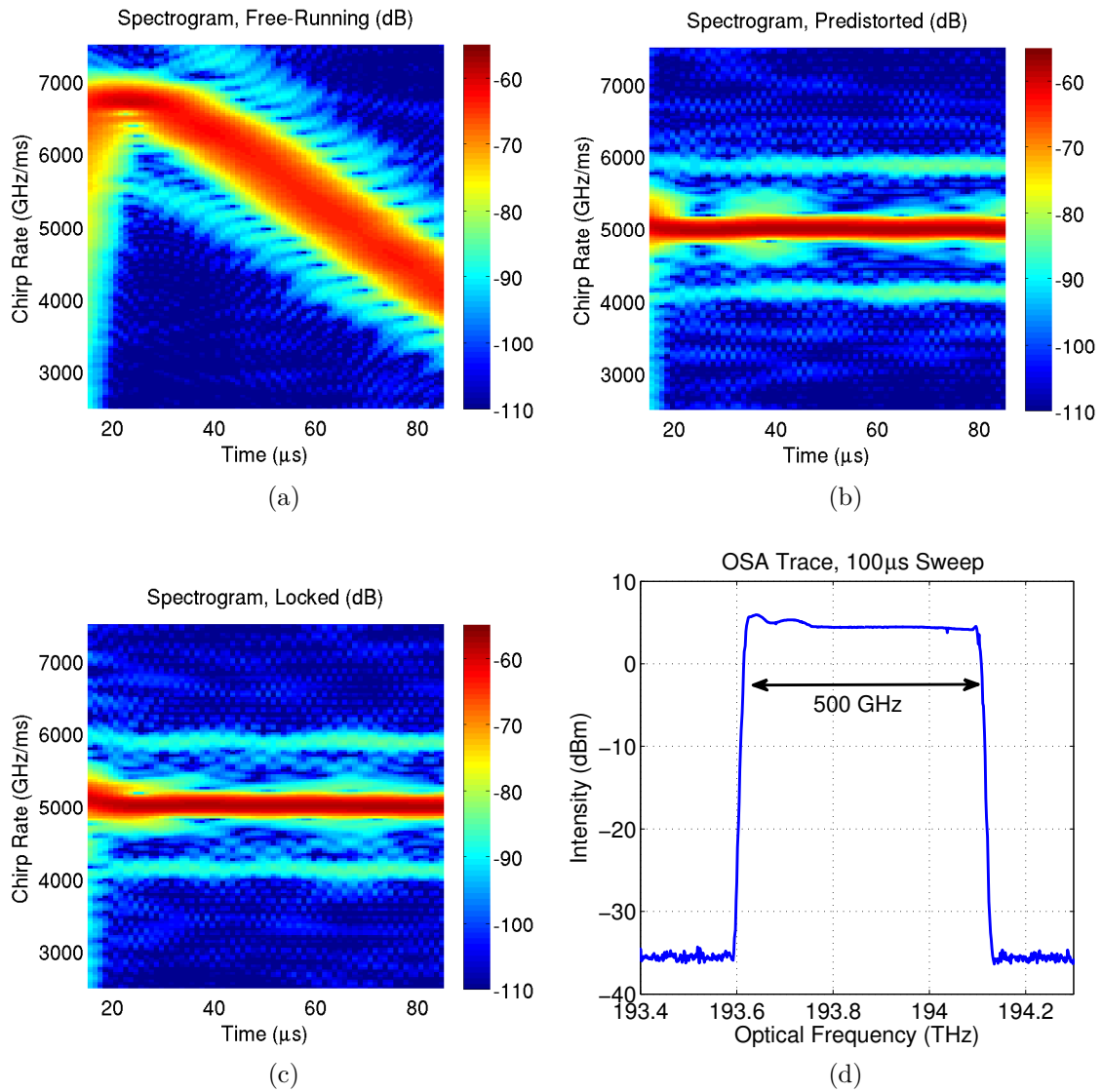


Figure 5.6. Experimental demonstration of generation of a perfectly linear chirp of 500 GHz / 0.1 ms using a VCSEL. (a), (b), and (c) Spectrograms of the optical chirp slope for a ramp input, after iterative predistortion and the phase-locked SFL respectively. (d) Measured optical spectrum.

We have therefore demonstrated the generation of precisely linear and broadband frequency sweeps of up to 5×10^{15} Hz/s and a chirp bandwidth of up to 500 GHz using a combination of laser current predistortion and an optoelectronic feedback loop. The rate of the optical frequency sweep is locked to and determined by the frequency of an external reference signal. The closed loop control system also reduces the inherent phase noise of the SCL within the loop bandwidth, thereby enabling coherent interferometry at larger distances. The chirp bandwidth and rate are mainly limited by the extent and speed of the thermal tuning of the frequency of the SCL.² We anticipate that tuning speeds larger than 10^{16} Hz/s are achievable using this technique. Other researchers have very recently demonstrated linearization of frequency chirps of external cavity lasers with a chirp bandwidth of about 5 THz [113], however the speed of the tuning was several orders of magnitude smaller than the frequency chirps demonstrated in this work.

5.3.2 Arbitrary Frequency Sweeps

The optoelectronic feedback technique can be extended to generate arbitrary frequency sweeps by the use of a VCO as the reference signal in figure 5.1. If the reference frequency, ω_R in equation (5.9), is varied with time, the optical frequency is given by

$$\omega_{SCL}(t) = \frac{1}{\tau} \int_0^t \omega_R(t) dt. \quad (5.14)$$

This principle was experimentally demonstrated by the generation of quadratic and exponential optical frequency sweeps using the DFB SCL, as shown in figures 5.7(a) and (b) respectively. In the former case, the reference frequency was varied linearly between 1.43 and 4.29 MHz over 1 ms. This corresponds to a linear variation of the optical frequency slope from 50 to 150 GHz/ms, and consequently, a quadratic variation of the optical frequency. In the latter case, the reference frequency was

²By “thermal tuning,” we mean the tuning due to a change in the device temperature, which is a consequence of a change in the injection current via joule heating.

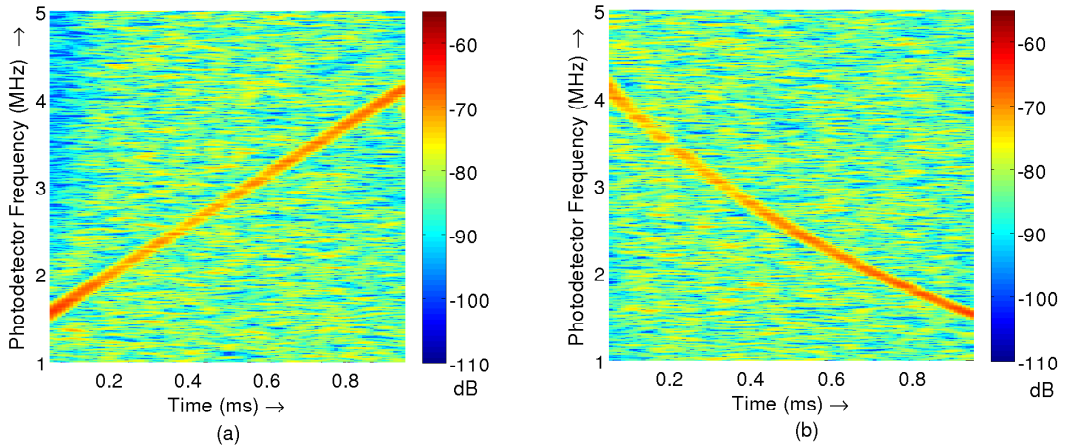


Figure 5.7. Measured spectrograms of the output of the loop photodetector, illustrating arbitrary sweeps of the SCL frequency. (a) The reference signal is swept linearly with time. (b) The reference signal is swept exponentially with time. The laser sweep rate varies between 50 and 150 GHz/ms.

varied exponentially between 4.29 and 1.43 MHz according to the relation

$$\omega_R(t) = 2\pi \times (4.29 \text{ MHz}) \times \left(\frac{1.43 \text{ MHz}}{4.29 \text{ MHz}} \right)^{t/(1 \text{ ms})}. \quad (5.15)$$

This corresponds to an exponential decrease of the slope of the optical frequency from 150 to 50 GHz/ms over 1 ms. A predistortion was applied to the integrator input in both cases, as described in section 5.2.2. The measured slope of the optical frequency sweep shown in figure 5.7 is identical to the temporal variation of the frequency of the reference signal. By predistorting the SCL current to produce the nominal output frequency sweep, this locking technique can be applied to generate any desired shape of the optical sweep.

5.4 Range Resolution of the Optoelectronic SFL

One of the most important applications of a linearly swept optical source is in FMCW reflectometry (see figure 1.2). The axial range resolution using a chirped wave with

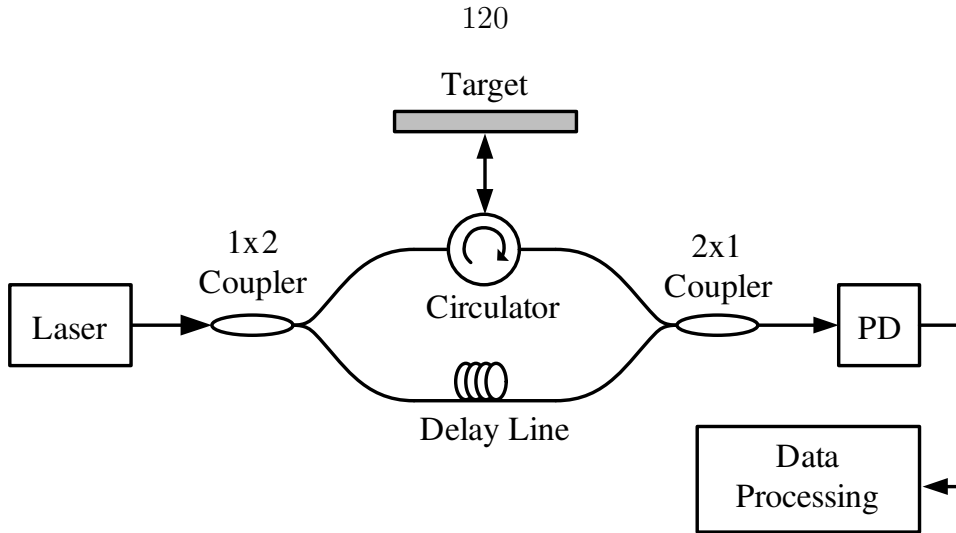


Figure 5.8. Schematic diagram of an FMCW ranging experiment with a linearly chirped optical source.

chirp bandwidth B (rad/s) is given by [54, 55]

$$\Delta d = \frac{\pi c}{B}, \quad (5.16)$$

where c is the speed of light, and a bandwidth of 500 GHz corresponds to a range resolution of 0.3 mm in air. The ability of the chirped VCSEL to resolve closely spaced targets was measured using the FMCW experimental setup shown in figure 5.8. Acrylic sheets of refractive index 1.5 and thicknesses varying from 1 to 6 mm were used as the target, and the reflections from the front and back surfaces were measured. A fiber delay line was used in the other arm of the interferometer to match the path lengths to about 0.5 m. The distance to the target was measured by computing the spectrum of the received photocurrent using a discrete-time Fourier transform.

The results of the measurement are shown in figure 5.9. From equation (5.16), the range resolution of this source is 0.2 mm in acrylic, though the practical resolution limit is 2 to 3 times this theoretical minimum resolution limit [55]. We see that the dual reflections at the smallest spacing of 1 mm are also perfectly resolved by the measurement. Range resolution measurements with smaller separations are discussed in the next chapter.

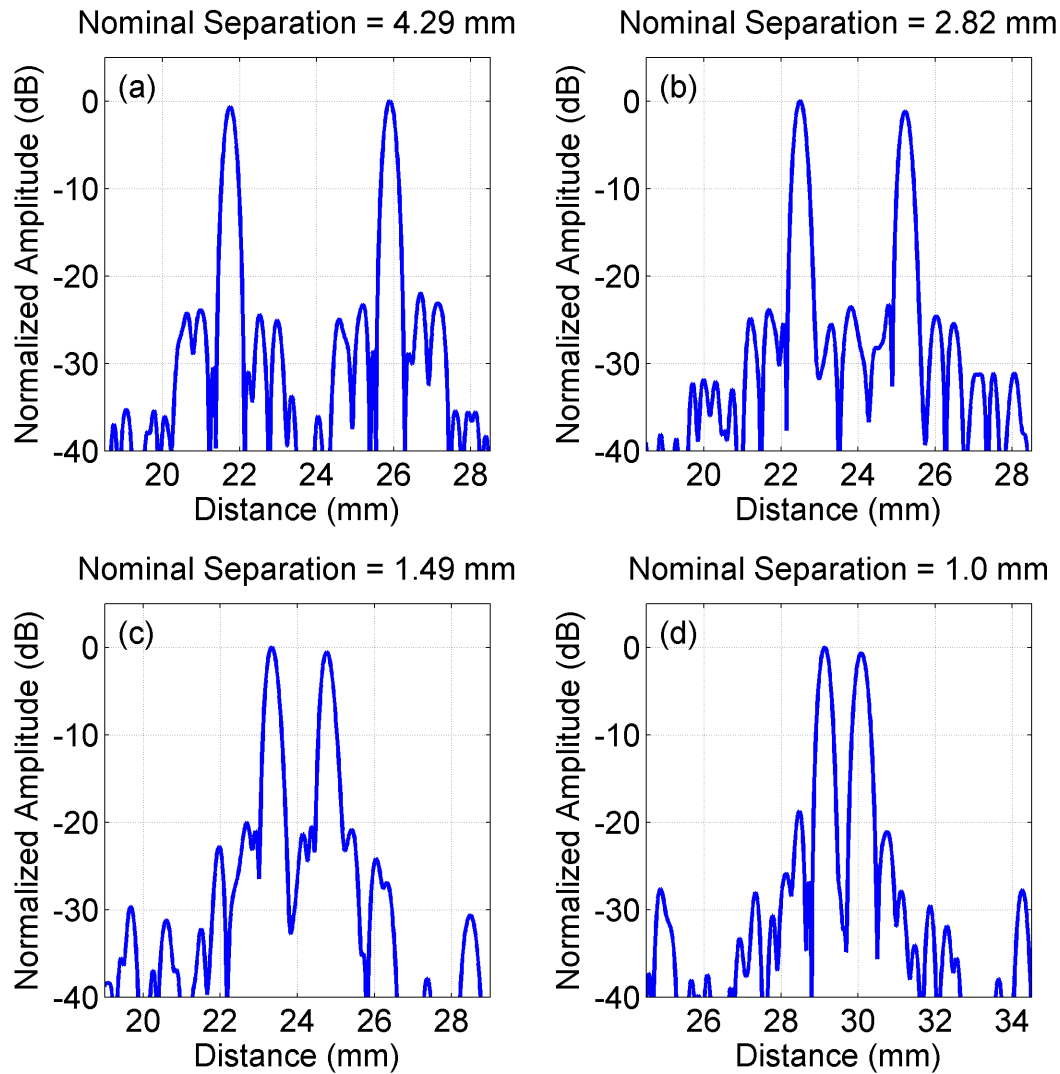


Figure 5.9. Range resolution measurements using the optoelectronic swept-frequency VCSEL. The target was an acrylic sheet of refractive index 1.5 and nominal thickness (a) 4.29 mm, (b) 2.82 mm, (c) 1.49 mm, and (d) 1.0 mm.

5.5 Label-Free Biomolecular Sensing Using an Optoelectronic SFL

Ranging experiments based on a linear swept-frequency optical source make use of the constant slope of the frequency chirp to determine the distance to the target, and the starting frequency of the sweep is not critical.³ The precise control over the starting frequency of the optical chirps ensures that the frequency profile is repeatable over multiple scans, and enables the use of the SFL in sensing and spectroscopic applications. In this section, we demonstrate the use of the optoelectronic SFL in liquid-phase label-free biomolecular sensing using a whispering gallery mode optical microtoroid resonator. We will limit ourselves to describing the salient features of the experiment and demonstrating that the SFL is particularly suitable for the application—detailed descriptions of sensor fabrication, chemical surface functionalization and the experimental setup are beyond the scope of this thesis.

Biomolecular assays that eliminate the need for labeling target biological molecules are very attractive for medical diagnostics since they can streamline the process and reduce the number of process steps as compared to traditional assays. Systems based on the measurement of surface plasmon resonances are already commercially available and have the ability to detect as little as 10 fg (10^{-14} g) of a target biomolecule material. In this work, we consider an alternative technique which is based on the measurement of the change in resonant frequency of a high-quality factor (Q) optical mode [114], specifically the whispering gallery mode of a silica microtoroid resonator [115]. The resonant frequency⁴ of the mode is measured by coupling light into the toroid using a tapered optical fiber [116] and measuring the transmission as a function of frequency. The surface of the resonator is functionalized using a chemical agent that selectively binds the target molecule of interest. The target molecule typically

³An exception is in the stitching of multiple swept-frequency sources, described in chapter 6.2

⁴Resonant wavelength shifts are typically reported in literature, whereas the optoelectronic SFL produces a perfectly linear chirp in optical frequency. We will refer to both the resonant wavelength and frequency in this section. The observed changes in the resonant frequency are small enough that they can be considered proportional to the changes in the resonant wavelength.

has a higher refractive index than the medium (water), and it therefore causes a small variation in the effective refractive index of the optical mode when it binds to the surface. The measurement of the resultant shift in the resonant wavelength can be used to quantitatively measure the concentration of the target molecule present in the solution, and sensitivities down to the single molecule level have been reported using this technique [117].

The optical resonant frequency is tracked using a tunable laser, and sensing experiments have almost universally used external-cavity mechanically tuned lasers for this purpose. These lasers suffer from two main drawbacks—their fast tuning range is typically much smaller than the free spectral range of the resonator, making it difficult to locate the resonance of interest; and the chirp is not necessarily linear, which constrains the measurement. The optoelectronic SFL developed in this work can overcome these limitations at a lower price and with improved robustness due to the lack of moving parts. The linewidth of typical DFB SCLs is ~ 1 MHz, which corresponds to a Q of $\sim 2 \times 10^8$ at 1550 nm. This implies that if the Q of the resonance is much lesser than 2×10^8 , the SFL behaves like a rapidly moving delta function that samples the optical resonance. The wide tuning range of the optoelectronic SFL helps to interrogate a large part of the free spectral range of the mode, making it easier to find the location of the resonance. In our experiments, we used SFLs with a tuning range of 100 GHz and a frequency chirp slope of 10^{14} Hz/s.

The measurement of a high- Q whispering gallery mode of a microtoroid in air at 1539 nm, shown in figure 5.10, demonstrates the ability of the laser to clearly resolve resonances with quality factors of 1.7×10^7 and 3×10^7 . The splitting of the resonance in figure 5.10 is attributed to coupling between the two counterpropagating modes of the resonator, which breaks their degeneracy. We note that if a stable resonator can be fabricated sufficiently high- Q , so that the resonance linewidth much smaller than the linewidth of the laser, the resonator can be used to measure the “linewidth” of the laser as its frequency is varied.⁵

⁵The “linewidth” of the chirped laser discussed here is more accurately the frequency resolution of the chirped laser.

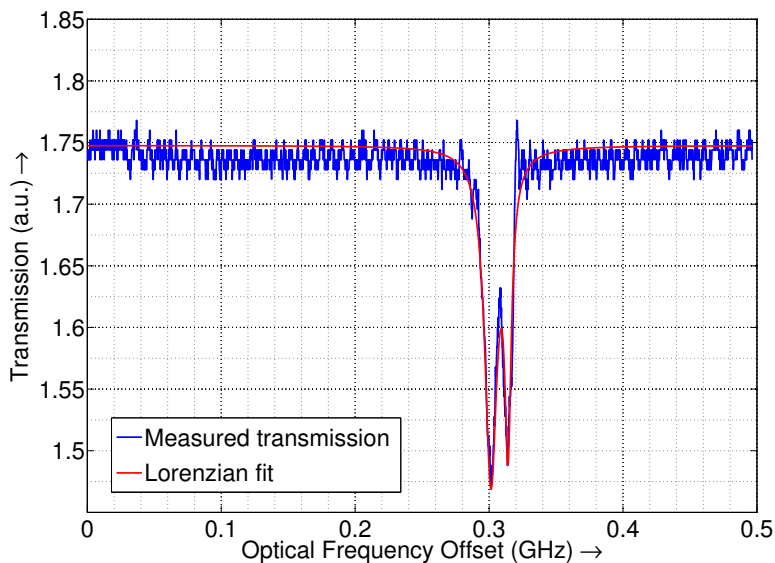
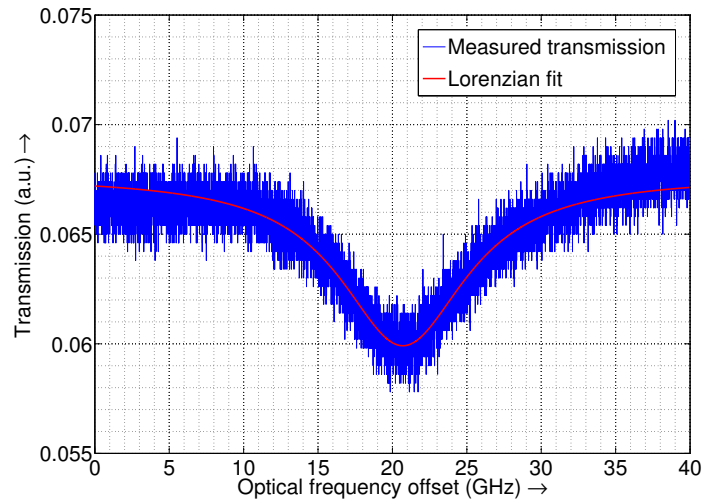


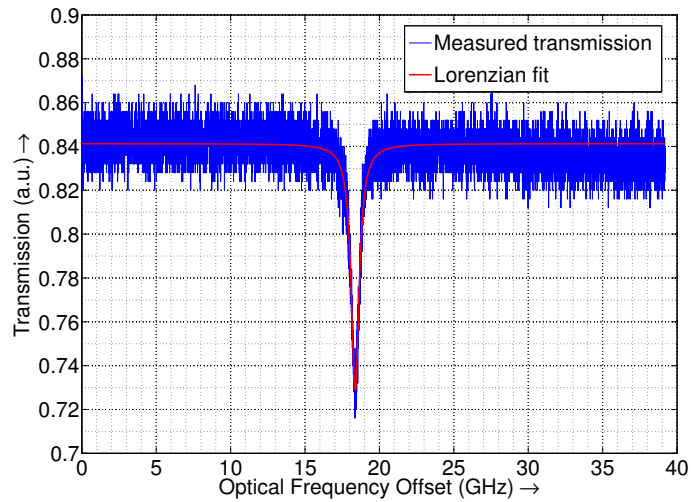
Figure 5.10. High- Q mode of a silica microtoroid in air, measured using an optoelectronic SFL at 1539 nm. The starting frequency of the sweep is subtracted from the x -axis. The splitting of the mode is attributed to scattering that couples degenerate counterpropagating modes and is resolved well by the measurement. From the Lorentzian fits, the quality factors of the modes are given by 1.7×10^7 and 3.3×10^7 .

The sensing of biologically relevant molecules requires that the resonator be immersed in water, since these molecules almost always exist in aqueous solution. However, water has a large absorption coefficient at telecom wavelengths, at which our lasers were originally developed. The large absorption in water of the evanescent tail of the optical mode significantly reduces the Q of the resonance. The best quality factors we measured across a large number (hundreds) of microtoroids in water at 1539 nm were limited to $\sim 2 \times 10^4$, as shown in figure 5.11(a), compared to best values of $\sim 2 \times 10^7$ in air. For this reason, liquid-phase sensing using optical resonators is typically performed at lower wavelengths toward the visible region of the optical spectrum. The absorption coefficient of water at 675 nm (4.2×10^{-13}) is much smaller than at 1300 nm (1.1×10^{-10}) and 1550 nm (1.3×10^{-9}) [118]. We therefore developed an optoelectronic SFL based on a DFB laser at 1310 nm, and using this SFL, measured quality factors of up to $\sim 4 \times 10^5$ at this wavelength for microtoroids in water, as shown in figure 5.11(b).⁶ Efforts are in progress to develop SFLs at even

⁶It is important to note that the measurements of figure 5.11 (a) and (b) were not performed



(a)



(b)

Figure 5.11. Whispering gallery mode resonances of a microtoroid in water, measured using optoelectronic SFLs at (a) 1539 nm and (b) 1310 nm. The starting frequency of the sweep is subtracted from the x -axis. From Lorentzian fits, the quality factors are measured to be 2.2×10^4 and 3.6×10^5 respectively.

lower wavelengths in the visible region, but the improvement of the quality factor by an order of magnitude to the 10^5 range already enables us to perform high-sensitivity biomolecular sensing experiments at 1310 nm.

We now present results of “specific” sensing of the molecule 8-isoprostane which is a marker for inflammation in exhaled breath. Concentrations of this biomarker are so low that, even when large volumes of breath condensate are collected (requiring a patient to breathe into the collection apparatus for 10 to 20 minutes), measurements remain near the detection limit [119, 120]. Improved sensitivity could reduce sample collection times and improve measurement confidence. The measurement is performed using a whispering gallery mode of a microtoroid resonator with a Q of 4.2×10^5 in water at 1310 nm. The measurement was performed by introducing known concentrations of the following solutions into a “flow cell” (volume $\lesssim 0.1$ mL) containing the microtoroid, at a constant flow rate of 50 $\mu\text{L}/\text{min}$ maintained using a syringe pump.

1. Protein G solution at 100 nM:⁷ This molecule binds to the surface of the silica microtoroid and provides binding sites for the adsorption of the antibody of interest.
2. Anti-8-isoprostane at 67 nM: This antibody binds to the protein G on the microtoroid surface, and provides binding sites for the detection of the target biomolecule.
3. 8-isoprostane, varying concentrations: When a solution containing different biomolecules is introduced into the flow cell, the 8-isoprostane molecules selectively bind to the anti-8-isoprostane on the resonator surface, enabling specific sensing.

using the same microtoroid; rather, they correspond to the typical largest quality factors measured among a large number (hundreds) of toroids. Variations in toroid fabrication necessitate the scouting of a large number of devices to find high- Q modes suitable for biosensing.

⁷A solution of concentration 1 M (1 molar) consists of one mole, or 6.023×10^{23} molecules, of the solute in one liter of the solution.

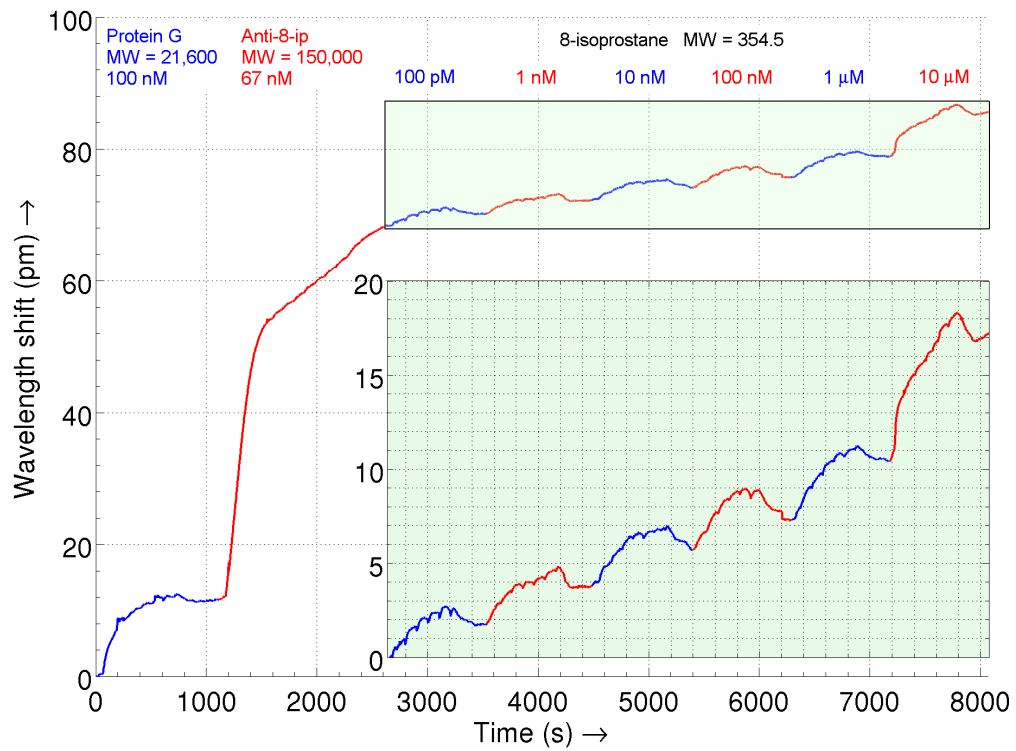


Figure 5.12. Specific sensing of 8-isoprostane using a microtoroid resonator and an optoelectronic SFL at 1310 nm. The quality factor of the resonance was 4.2×10^5 , and the flow rate was $50 \mu\text{L}/\text{min}$.

The resultant shifts in the resonant wavelengths were recorded and are plotted in figure 5.12. Protein G and Anti-8-isoprostane are large molecules (molecular weights of 21,600 and 150,000 respectively, as listed in the figure), and therefore result in large resonant shifts. The introduction of different concentrations of the small target molecule, 8-isoprostane, results in different values of shift in the resonant wavelength. These preliminary experiments demonstrate the ability of this sensor to measure concentrations of the analyte at least as low as 100 pM. The small physical size of the molecule results in very small wavelength shifts, but these can be resolved by the measurement. Further studies are necessary to determine the detection limit and the dynamic range of the sensor. Studies are also in progress to analyze the effects of fluid flow across the toroid and the resultant heat transfer away from the toroid, on the resonant wavelength.

We note that the measurement described above was performed using a resonance with a Q of “only” 4.2×10^5 , and does not fully harness the advantages of low scattering losses in a reflow microtoroid resonator [115]. This implies that other, more convenient, resonator configurations can be used to perform measurements with similar sensitivity—in particular, integrated waveguide-resonator configurations lithographically fabricated on a single chip. Such devices will not require the extremely precise alignment of a tapered fiber to couple light into the resonator, and have the potential to enable the sensor to progress from merely a complex laboratory demonstration to a practically feasible and useful device.